Determination of the Stereochemistry of 3-Hydroxymethyl-2,3-dihydro-[1,4]dioxino[2,3-*b*]-pyridine by Vibrational Circular Dichroism and the Effect of DFT Integration Grids

T. Kuppens,[†] W. Langenaeker,[‡] J. P. Tollenaere,[§] and P. Bultinck*[,†]

Department of Inorganic and Physical Chemistry, Ghent University, Krijgslaan 281-S3, B-9000 Gent, Belgium, Department of Molecular Design and Chemoinformatics, Johnson & Johnson Pharmaceutical Research and Development, Turnhoutseweg 30, B-2340 Beerse, Belgium, and Department of Medicinal Chemistry, Utrecht University, Sorbonnelaan 16, NL-3508 TB Utrecht, The Netherlands

Received: August 7, 2002; In Final Form: October 23, 2002

Vibrational circular dichroism (VCD) spectra are presented for 3-hydroxymethyl-2,3-dihydro-[1,4]dioxino-[2,3-*b*]pyridine. The assignment of the stereochemistry has been done by comparison between the experimental spectra and theoretically calculated spectra for both enantiomers. The DFT calculations were found capable to correctly assign absolute configurations. The influence of the basis set used in the DFT calculations on the extent of the agreement between the theoretical and experimental findings was investigated by use of different Pople-style basis sets and correlation consistent basis sets, showing that 6-31G* is an acceptable basis set, and that cc-pVTZ yields the best agreement. Similarly, the effect of DFT integration grids was examined. A quantitative measure for the similarity between experimental and theoretical spectra is used.

Introduction

It is well-known that optical isomers may demonstrate a different biological activity.[1] Therefore, in the pharmaceutical industry, the knowledge of the absolute configuration is of the utmost importance. Among several methods available to determine the absolute configuration, X-ray diffraction (XRD) is often the method of choice because it yields the most reliable results. This relatively labor-intensive method, however, requires the availability of well-defined crystals and the presence of "heavy" atoms, which is often a problem. A second popular method, Nuclear Magnetic Resonance (NMR), is not always applicable either. Often specific methods have to be applied to eliminate the degeneracy of the enantiomers, e.g., the use of chiral solvents or chiral shift-reagents. These methods are sometimes troublesome or not working and may give contradictory results.[2−4] Retro-synthesis also has several drawbacks, and is usually labor-intensive.

A technique that holds great promise for the determination of the absolute configuration and gains importance quite rapidly, is the measurement of Vibrational Circular Dichroism (VCD). This technique is based on the differential absorption by the sample of left and right circularly polarized infrared (IR) radiation. Since circularly polarized light (CPL) itself has handedness, different interactions of the two forms of light occur with chiral molecules, i.e., the differential CPL absorptions of two enantiomers are opposite in sign.

For VCD to be applicable, the acquired spectra should be interpretable. However, interpretation of VCD spectra is not straightforward and it requires an algorithm that relates both the structure and spectra. Hence the necessity to predict spectra for different stereoisomers. By comparison of the predicted spectrum with the experimental spectrum, identification of the stereoisomer present in solution is possible. The main issue in the calculation of the theoretical spectra is the sign of the differential transitions and the prediction of the rotational strength, which is proportional to the area under the VCD band. A reliable quantum chemical method for molecules of variable size was developed by Stephens et al. in 1996.[5] Several studies have already illustrated the applicability of this method in determining the absolute configuration of a molecule.[6,7]

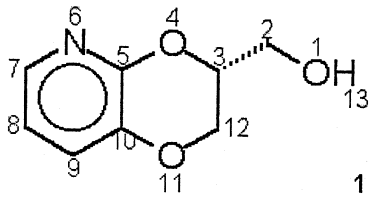

1

Figure 1. R(+)-3-hydroxymethyl-2,3-dihydro-[1,4]dioxino[2,3-*b*]pyridine ≡ *R*(+)-**1**.

From an experimental point of view, VCD exhibits several important advantages. VCD spectra can be measured almost routinely, nowadays, using specially adapted IR spectrometers. An even more important advantage over XRD techniques is that measurements are possible in solvents, i.e., there is no need for crystals or "heavy" atoms.

In this study, the absolute configuration of 3-hydroxymethyl-2,3-dihydro-[1,4]dioxino[2,3-*b*]pyridine, **1**, shown in Figure 1 is known by its synthesis route.[8] The *R* enantiomer corresponds to the sample with a positive optical rotation, the *S* enantiomer to the one with a negative optical rotation.

VCD spectra have been recorded for both the *R* and *S* enantiomer. Both spectra were made available for the authors of the present study without revealing what spectrum corresponds to what enantiomer. DFT calculations were used to calculate VCD spectra for both the *R* and *S* enantiomers, and by comparison between the available experimental and theoretical spectra, an assignment was made. This assignment was then checked against the knowledge of the synthesizing chemists. The first aim of the present study is to find out whether these assignments can be made correctly.

[†] Department of Inorganic and Physical Chemistry.
[‡] Department of Molecular Design and Chemoinformatics.
[§] Department of Medicinal Chemistry.

10.1021/jp021822g CCC: $25.00
Published on Web 01/04/2003

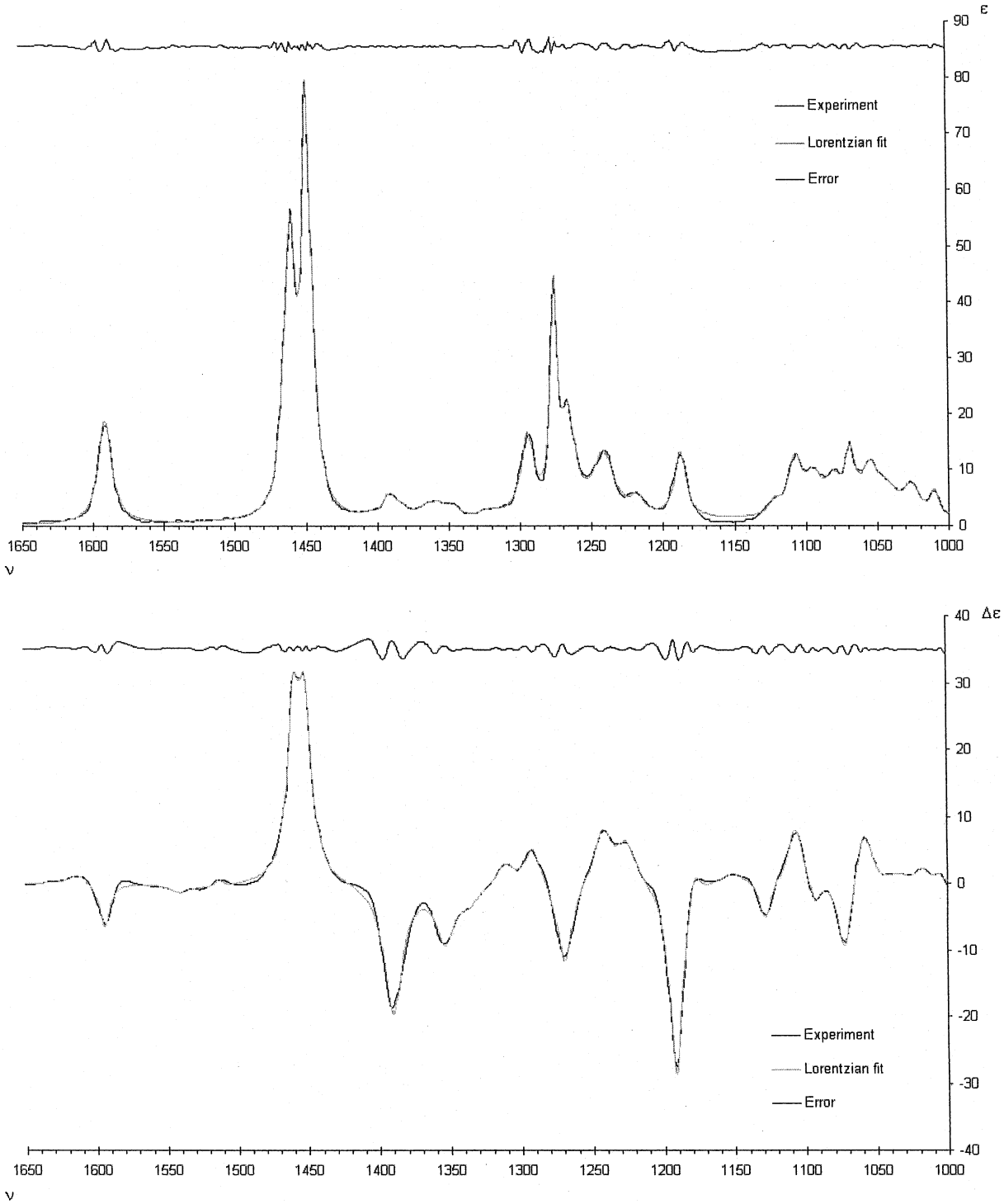

Figure 2. Unpolarized IR absorption spectrum (a) and VCD spectrum (b) for *R*(+)-**1**, including Lorentzian fit and error (absorptions and differential absorptions in absorbance units).

Another objective is to investigate the effects of the DFT integration grid on calculated VCD properties. A question that may be raised is whether it is possible to make approximations to the calculation so these become less expensive, affecting only to little extent the quality of the simulated VCD spectra.

Experimental Section

The *R* and *S* enantiomers of **1** were obtained with a minimal 98%EE. Synthesis routes were previously described in the literature.[8,9] The unpolarized IR and VCD spectra for both enantiomers of **1** were recorded in a 90 μm CaF_2 cell on a Bruker IFS 66/S FTIR spectrometer using a *PMA 37* module. The unpolarized absorption spectra have a resolution of 2 cm^{-1} and a recording time of 25 s each. The resolution of the VCD spectra is 6 cm^{-1} with recording times of 3 h each. Samples of **1** were dissolved in $CDCl_3$ at a concentration of 0.27 M. The spectral window was set to 1000−1650 cm^{-1}. Experimental spectra of the *R*(+)-sample are shown in Figure 2.

Computational Methodology

Multiple conformations of **1** are possible, each conformation contributing to the IR absorption and VCD spectrum of the

molecule. As calculated spectra are heavily dependent on the molecular conformation,[10] a thorough conformational analysis is needed.

To find the different minimum energy conformations of the molecule a two-way conformational analysis approach is used. In the first approach, B3LYP/6-31G* calculations are used. The pyridine ring is considered rigid, whereas the dioxane ring, as well as all other fragments, are considered flexible. The dihedral angles are developed in a 60° grid. Not all resulting structures are chemically sound, and prior to initiating a geometry optimization the search tree is pruned by application of a bump check and ring constraints. The remaining conformations are then optimized on the B3LYP/6-31G* level. The resulting minima are collected for further geometry optimizations and spectroscopic calculations.

A major problem with systematic searches is the combinatorial explosion, which hampers systematic searches for larger molecules (more dihedral angles) and finer dihedral angle grids. The computational requirements of DFT calculations are such that finer grids are not possible in the systematic search. We therefore also used a stochastic search using the MM3 force field.[11]

This method, as implemented in the MM3(96) program, optimizes a geometry of the molecule and randomly moves ("kicks") the atoms in an atom-centered predefined sphere. The new structure is then again optimized, yielding a new or possibly previously located stationary point, after which the geometry of this new stationary point is kicked. Our routines are used, to automate the entire search and check for convergence. The conformational search is considered converged if all minima with a relative energy—compared to the global minimum—below 20 kcal/mol are found more than 20 times and a new stochastic search does not yield any new minima.[12] Our routines also remove redundant structures by compiling the lists of stationary points, from different stochastic searches.

DFT molecular geometries were obtained by the minimization of the MM3 geometries of the stationary points found during the MM3 conformational search. These were supplemented with the B3LYP/6-31G* geometries from the ab initio conformational analysis. DFT calculations are performed with GAUSSIAN98, revision A.6,[13] using the B3LYP hybrid density functional[14,15] and DZ and TZ Pople basis sets with polarization, i.e., 6-31G, 6-31G*, 6-31G** and 6-311G**.[16] The cc-pVDZ, cc-pVTZ and cc-pVQZ Dunning basis sets are also applied. Default GAUSSIAN98 basis set parameters are used.

For the geometry optimization and the calculation of the spectroscopic properties different integration grids are applied. Euler−Maclaurin−Lebedev grids of the type (*mm*,*nnn*) are used, having *mm* radial shells and *nnn* angular points per shell. Pruned[17] versions of these grids are also applied. In the latter the number of angular points varies with the shell with a maximum of *nnn* on radii that are relevant for chemical bonding.[18] The default grid in GAUSSIAN98 is a pruned version of the (75,302) grid further denoted as (75,302)p, invoked with the keyword GRID=FineGrid. The (50,194)p grid[17] is invoked with the keyword GRID=SG1Grid and the (35,110)p grid with GRID=CoarseGrid.[19]

Gauge-including atomic orbitals (GIAO) are used to calculate atomic axial tensors (AAT).[5] Together with harmonic force fields and atomic polar tensors (APT) the rotational strengths are calculated.[20,21]

For each DFT energy minimum in the potential surface the dipole and rotational strengths are calculated. The resulting line spectra are then broadened using a Lorentzian band shape, giving single conformer spectra. For the total frequency range, the total "broadened" dipole and rotational strength is calculated as the weighted sum of the single conformer spectra (eq 1a,b). In other words, the IR absorption and VCD spectrum of a molecule is computed as a linear combination of the spectra for the different conformations.

$$D_{\mathrm{tot}}(\nu) = \sum_A F(A) D_A(\nu) \tag{1a}$$

$$R_{\mathrm{tot}}(\nu) = \sum_A F(A) R_A(\nu) \tag{1b}$$

$F(A)$, being the population of conformer A, is calculated assuming a Boltzmann distribution (eq 2):

$$F(A) = \frac{e^{-H_A^0/RT}}{\sum_i e^{-H_i^0/RT}} \tag{2}$$

where i runs over all conformers. We omit the entropic contributions to the Gibbs free energy and, consequently, use the enthalpy to calculate the conformational populations. The enthalpy is calculated via DFT using the standard thermochemical expressions and under the usual assumptions.[22]

To discuss the similarity of spectra a quantitative measure has to be introduced. We use a measure based on the overlap integral, i.e.,

$$S = \frac{\int f(\sigma\nu) g(\nu) d\nu}{\sqrt{\int f^2(\sigma\nu)\, d\nu \int g^2(\nu)\, d\nu}} \tag{3}$$

f and g are the functions that represent the spectral intensities at each frequency ν.

Identical spectra have an overlap integral equal to 1. For unpolarized IR spectra, with no negative values, the overlap integral tends to 0 when the similarity diminishes. For VCD spectra however the overlap can become negative, and S is equal to -1 when the spectra are the opposite of each other, i.e., when both spectra are from enantiomers. Frequency scaling is introduced by factor σ.

Experimental IR absorption and VCD spectra are Lorentzian fitted to calculate the experimental dipole and rotational strengths via following relations:[23]

$$D_i = 9.18 \times 10^{-39} \int \epsilon_i \frac{d\nu}{\nu}$$

$$R_i = 2.29 \times 10^{-39} \int \Delta\epsilon_i \frac{d\nu}{\nu} \tag{4}$$

Here, ϵ and $\Delta\epsilon$ are the IR absorption and differential absorption in L mol^{-1} cm^{-1}. D and R are in esu^2 cm^2.

Results and Discussion

Conformational Analysis. Conformational isomers of **1** differ by (a) the orientation of the exocyclic bond [O11−C12−C3−C2,τ_1], i.e., pseudoequatorial or pseudoaxial, (b) the rotameric dihedral angle about the C2−C3 bond τ_2, and (c) the rotameric dihedral angle about the O1−C2 bond τ_3.

The position of the exocyclic substituent—the methylhydroxyl group—is either designated as "eq" or "ax". Assuming three typical minima in the torsion potential energy, i.e., for dihedral angles of 60, 180, and −60°, the dihedral angles are character-

TABLE 1: MM3 Minima, Conformation Description, and Relative MM3 Energy (RE, in kcal/mol) Together with Key Dihedral Angles (τ_1, τ_2, and τ_3, in Degrees)

	notation	RE(MM3)	τ_1, $O_{11}-C_{12}-C_3-C_2$	τ_2, $O_4-C_3-C_2-O_1$	τ_3, $C_3-C_2-O_1-H_{13}$
1	eqGg′	0.00	179	63	−54
2	eqG′g	0.08	178	−61	58
3	axGg′	0.64	−59	61	−57
4	eqG′t	1.60	176	−68	170
5	eqTt	1.63	179	179	−177
6	eqGt	1.80	178	69	−172
7	axG′g	1.84	−67	−68	39
8	axGt	2.43	−59	69	−169
9	axTt	2.45	−60	177	179
10	axG′t	4.72	−67	−68	170

TABLE 2: Relative Energies (in kcal/mol) for the Minima, the Conformation Description, and MM3 Energy Ranking[a]

	notation	6-31G*	6-31G**	6-311G**	cc-pVDZ	cc-pVTZ
2	eqG′g	0.00	0.00	0.00	0.00	0.00
1	eqGg′	0.81	0.84	0.81	0.85	0.55
3	axGg′	1.60	1.61	1.60	1.63	1.55
5	eqTt	2.49	2.49	2.06	2.56	1.78
9	axTt	2.94	2.91	2.52	2.90	2.40
4	eqG′t	3.59	3.54	3.21		
7	axG′g	4.28	4.30	4.14		
6	eqGt	4.96	4.92	4.47		
8	axGt	5.41	5.36	4.97		

[a] For the cc-pVDZ and cc-pVTZ basis set only, the five lowest energy conformations were minimized.

TABLE 3: MM3 Ranking, Conformation Description, and Relative B3LYP/6-31G* Energy (RE, in kcal/mol) and Optimized Key Dihedral Angles (τ_1, τ_2, and τ_3, in Degrees)

	notation	RE	τ_1, $O_{11}-C_{12}-C_3-C_2$	τ_2, $O_4-C_3-C_2-O_1$	τ_3, $C_3-C_2-O_1-H_{13}$
2	eqG′g	0.00	−177.1	−60.4	58.0
1	eqGg′	0.81	−178.4	58.1	−53.4
3	axGg′	1.60	−64.1	56.1	−52.2
5	eqTt	2.49	−178.9	176.6	−178.7
9	axTt	2.94	−65.2	171.4	174.5
4	eqG′t	3.59	178.5	−74.3	163.2
7	axG′g	4.28	−69.7	−59.0	70.3
6	eqGt	4.96	179.6	73.2	−162.3
8	axGt	5.41	−63.5	68.4	−162.5

ized as G, T, and G′ respectively for gauche clockwise, trans, and gauche counterclockwise C−C bond torsion, and similarly g, t, and g′ for the O−C bond torsion.

The conformational searches yielded 10 stationary points, all corresponding to minima on the MM3 PES. These are shown in Figure 3. Table 1 shows their corresponding notation and relative MM3 energies together with values for τ_1, τ_2, and τ_3.

All 10 minima were used as starting geometries for geometry optimizations using the B3LYP functional and the different basis sets mentioned above. These geometry optimizations were not straightforward. Through application of constrained geometry optimizations, we succeeded in locating most minima with the different Pople basis sets. A common feature for these basis sets is the fact that no axG't structure could be located. The

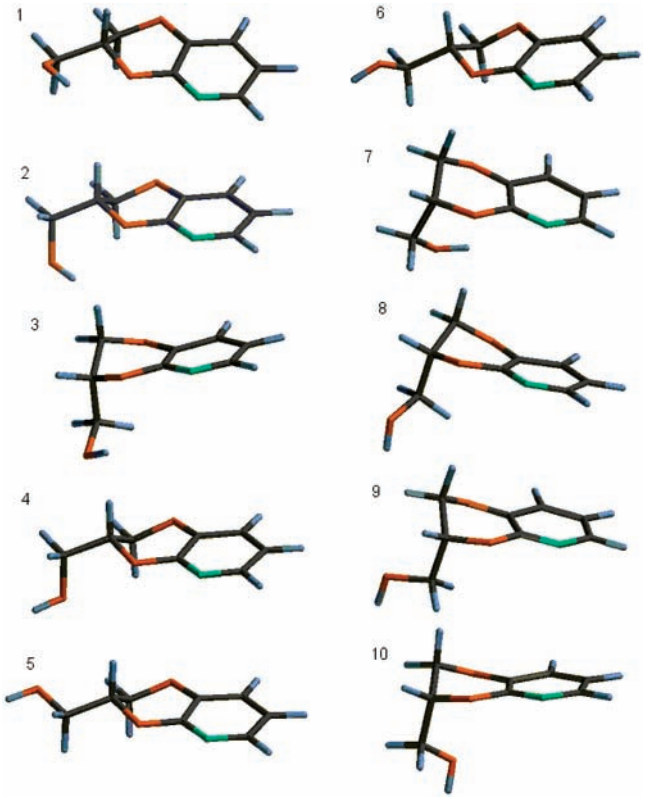

Figure 3. Visualization and notation of the PES minima for *R*(+)-**1**. Conformation numbering conforms to that of Table 1.

6-31G basis set was found to be severely lacking in giving a good description of the molecular PES. Given the conformation dependence of the VCD spectra, this basis set was considered inapplicable for our purposes, and thus excluded from the further calculations. For the cc-pVDZ and cc-pVTZ basis set only conformations with a relative energy below 3 kcal/mol (according to 6-311G**) were minimized.

A summary of the results of these different geometry optimizations is presented in Table 2. Tables 1 and 2 clearly show that the relative energies of the different structures differ

TABLE 4: Relative Energies (in kcal/mol) for the Minima, Using Different DFT Integration Grids (B3LYP/6-31G*, Including Geometry Optimization with Each Grid)

MM3 nr	notation	(35,110)p	(50,194)p	(75,302)p	(50,302)	(75,194)	(75,434)	(99,302)
2	eqG′g	0.00	0.00	0.00	0.00	0.00	0.00	0.00
1	eqGg′	0.69	0.83	0.81	0.80	0.84	0.82	0.80
3	axGg′	1.91	1.56	1.60	1.60	1.56	1.59	1.59
5	eqTt	2.42	2.52	2.49	2.48	2.54	2.49	2.48
9	axTt	2.90	2.91	2.94	2.94	2.92	2.96	2.94
4	eqG′t	3.48	3.60	3.59	3.59	3.60	3.59	3.59
7	axG′g	4.22	4.33	4.28	4.26	4.33	4.28	4.26
6	eqGt	4.70	4.97	4.96	4.95	4.98	4.96	4.95
8	axGt	5.64	5.39	5.41	5.41	5.38	5.40	5.40

TABLE 5: B3LYP/6-31G* Optimized Dihedral Angles (τ_1, τ_2, and τ_3, in Degrees) for Conformation eqGg′ and Relative Energies (RE, in μhartree) with Respect to the (99,974) Grid

DFT grid	RE	τ_1, $O_{11}-C_{12}-C_3-C_2$	τ_2, $O_4-C_3-C_2-O_1$	τ_3, $C_3-C_2-O_1-H_{13}$
(35,110)p	189.07	−178.0	59.6	−53.4
(50,194)p	−13.58	−178.4	58.1	−53.8
(75,302)p[a]	16.58	−178.4	58.1	−53.8
(50,194)	−20.19	−178.3	58.1	−53.3
(50,302)	21.92	−178.4	58.0	−53.3
(50,434)	6.96	−178.4	58.0	−53.3
(50,974)	9.51	−178.4	58.2	−53.7
(75,194)	−27.24	−178.4	58.1	−53.2
(75,302)	14.68	−178.4	58.1	−53.3
(75,434)	−0.48	−178.4	58.0	−53.2
(75,974)	1.63	−178.4	58.0	−53.2
(99,194)	−28.49	−178.4	58.2	−53.7
(99,302)	12.96	−178.4	58.1	−53.2
(99,434)	−1.89	−178.4	58.1	−53.2
(99,974)	0.00	−178.4	58.0	−53.2

[a] GAUSSIAN98 default grid.

TABLE 6: Maximized Overlap Integrals S_{max} and Optimal Scaling Factor σ_{max} Relative to the B3LYP/cc-pVQZ Broadened Spectra for the eqGg′ Conformation

		6-31G	6-31G*	6-31G**	6-311G**	cc-pVDZ	cc-pVTZ
IR	S_{max}	0.818	0.841	0.775	0.835	0.750	0.960
	σ_{max}	0.9975	0.9888	0.9919	1.0000	0.9939	0.9992
VCD	S_{max}	0.356	0.563	0.537	0.586	0.303	0.701
	σ_{max}	0.9971	0.9879	0.9928	0.9985	1.0000	0.9994

quite strongly between the MM3 and DFT levels of theory. The energetic ordering of the minima also undergoes a number of changes. Most notably, on the MM3 level, the structures with an equatorial exocyclic bond were lower in energy than those with an axial exocyclic bond (except for the axGg′ structure). On the DFT level there is no longer such a clear distinction between both types of structures. The relative energies found using the 6-31G* and 6-31G** basis sets differ little, but when going to the 6-311G** basis set, the energetic spread of the minima is reduced. This effect is also found when going from the cc-pVDZ to the cc-pVTZ basis set. As mentioned above, the 6-31G basis set yields fewer minima, and for those that were found, the relative energies differ strongly from the more extended basis sets (data not shown).

Table 3 gives the dihedral angles τ_1, τ_2, and τ_3 for the optimized geometries using the 6-31G* basis set. Comparison with Table 1 clearly shows that the dihedral angles in the MM3 structures agree quite well with the DFT values.

Table 4 gives the relative energies using different DFT integration grids. Only small differences between the different grids are found, with the exception of the (35,110)p grid. The extent of the difference between the (35,110)p grid and the other grids also differs depending on the conformation involved.

Table 5 gives the energy difference (in μhartree) for the eqGg′ conformer relative to the (99,974) energy. Again, only minor effects are seen, except for the (35,110)p grid, where the deviation is an order of magnitude larger. Geometries (expressed through τ_1, τ_2 and τ_3) differ very little between the different grids, again except for the (35,110)p grid.

Single Conformation. Basis set dependence for the calculated spectra was studied. Vibrational frequencies calculated with various basis sets, scale differently with respect to each other. A maximization of the overlap integral S was carried out by varying the scale factor σ in eq 3, taking the cc-pVQZ basis set as reference. In Table 6 S_{max} and σ_{max} are given for the eqGg′ conformation, both for the IR absorption and VCD spectra.

The smallest basis set used, i.e., 6-31G produces an IR absorption spectrum that has a large overlap with the cc-pVQZ IR spectrum. However, this overlap integral is fortuitously large; both spectra differ significantly from each other. For the eqGg′ single conformer VCD spectra, the performance of the 6-31G basis set is poor compared to the larger basis sets (Table 6), again indicating the 6-31G set to be of little use for our purposes. This agrees with the findings of Stephens et al.[6] The performance of the cc-pVDZ basis set is also inferior to comparable basis sets. The cc-pVTZ basis set stands out above the other.

One may expect properties calculated with denser grids to be more accurate than those calculated with smaller, less dense grids. The IR absorption and VCD overlap integrals with $\sigma = 1$ for the eqGg′ conformer are calculated with the (99,974) grid spectra as reference, and are given in Table 7. The grids with 194 angular points have a performance that is less compared to the other grids with the same number of shells. The overlap integrals for the VCD and IR absorption spectra calculated with 50 radial shell grids are all surprisingly high. This seems to be

TABLE 7: Correlation Coefficient (in Percent) and Overlap Integrals S ($\sigma = 1$) Relative to the (99,974) Grid of the Broadened Unpolarized IR Absorption and VCD Spectra for Conformation eqGg′

DFT grid	correlation coefficient D, %	correlation coefficient R, %	S_{IR}	S_{VCD}	relative CPU
(35,110)p	93.56	94.96	0.824	0.647	0.5
(50,194)p	99.71	99.67	0.985	0.972	0.7
(75,302)p[a]	99.99	99.98	0.998	0.997	1.0
(50,194)	99.63	99.66	0.988	0.977	1.8
(50,302)	99.86	99.96	0.993	0.987	2.6
(50,434)	99.90	99.94	0.985	0.978	3.2
(50,974)	99.84	99.93	0.996	0.993	7.2
(75,194)	99.91	99.86	0.955	0.930	2.5
(75,302)	99.99	99.98	1.000	0.999	3.7
(75,434)	99.99	99.99	0.995	0.993	5.0
(75,974)	100.00	99.99	1.000	1.000	11.3
(99,194)	99.88	99.84	0.951	0.921	3.1
(99,302)	99.99	99.98	1.000	0.999	4.3
(99,434)	100.00	99.99	0.997	0.996	5.7
(99,974)	100.00	100.00	1.000	1.000	13.4

[a] GAUSSIAN98 default grid.

TABLE 8: Relative Single Point B3LYP/6-31G* Energies (in kcal/mol) for the eqG′g Equilibrium Geometry, Correlation Coefficient (in Percent) of the Dipole, and Rotational Strength and Overlap Integrals S ($\sigma = 1$) with Respect to the Standard Orientation for Three Different Orientations and the (50,194)p and (75,302)p Grids[a]

(50,194)p

	RE	correlation coefficient D, %	correlation coefficient R, %	S_{IR}	S_{VCD}
10*x*[b]	−0.0096	99.35	99.42	0.977	0.916
				0.991[c]	*0.974*
20*x*	0.0248	97.03	97.71	0.959	0.926
				0.992	*0.980*
20*x*30*y*	0.1079	99.02	97.58	0.933	0.893
				0.947	*0.926*

(75,302)p

	RE	correlation coefficient D %	correlation coefficient R %	S_{IR}	S_{VCD}
10*x*	−0.0049	99.67	99.75	0.995	0.992
				0.999	*0.996*
20*x*	0.0052	99.86	99.92	0.999	0.998
				1.000	*0.999*
20*x*30*y*	0.0027	99.86	99.88	0.993	0.989
				0.996	*0.991*

[a] The overlap integrals are given for two frequency intervals, i.e., 300−2000 cm^{-1} and 1000−2000 cm^{-1}. [b] Orientations are described in the text. [c] Overlap integrals are given for two frequency intervals. The first value is for the 300−2000 cm^{-1} interval and the second (in italic) for the 1000−2000 cm^{-1} interval.

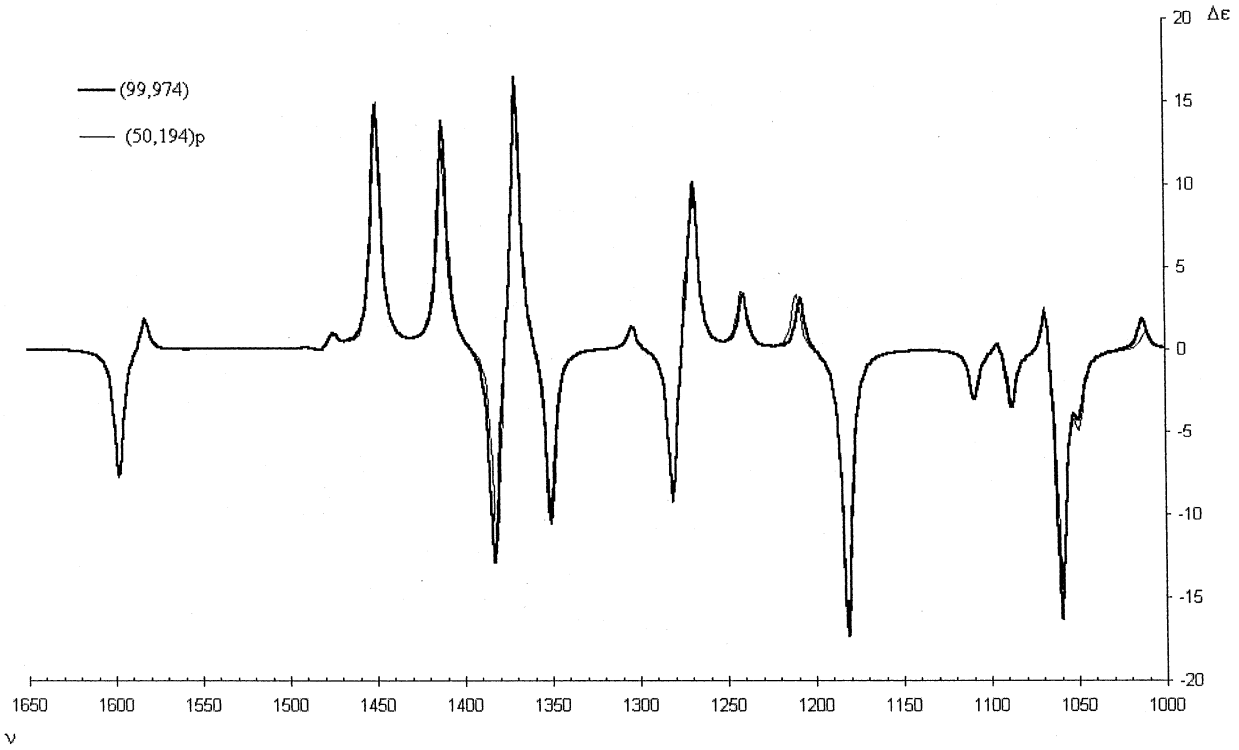

Figure 4. VCD spectra of conformer eqGg′ for the (50,194)p and (99,974) reference grid (VCD intensities in 10^{-44} esu^2 cm^2, frequencies in cm^{-1}).

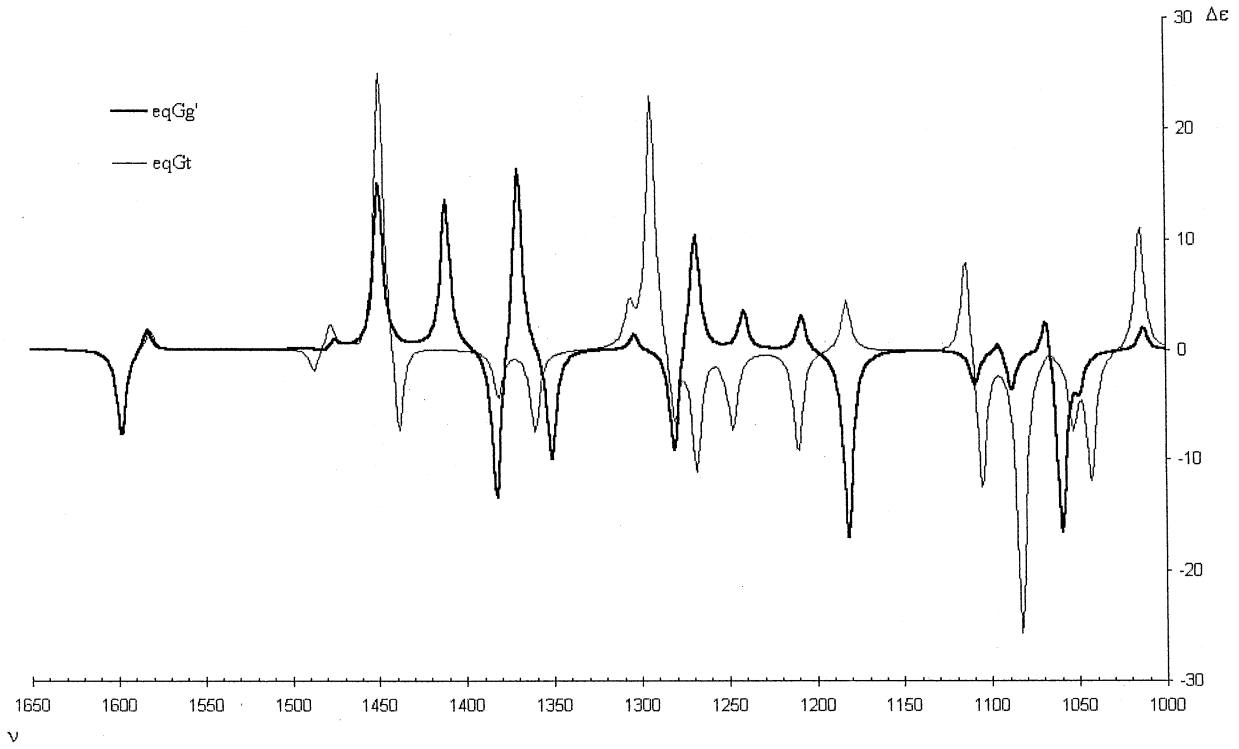

Figure 5. Single conformer spectra of eqGt and eqGg′ calculated at B3LYP/6-31G* level and the (75,302)p grid (VCD intensities in 10^{-44} esu^2 cm^2, frequencies in cm^{-1}).

an artifact, attributed to a small but conspicuous frequency shift of the peak at approximately 448 cm^{-1} (mode 9b: O−H out-of-plane bending vibration) {note: Vibrational modes are denoted with the fundamental number (based on the calculation) and the corresponding conformation, i.e., a ≡ eqG′g, b ≡ eqGg′ c ≡ axGg′, d ≡ eqTt.} relative to the (99,974) grid. For the (75,194) and (99,194) grids this relative shift is bigger than for the (50,194) grid (respectively 4.48 and 4.98 against 1.60 cm^{-1}). Because of the considerably high dipole and rotational strengths of mode 9b these shifts have a substantial effect on the overlap integral. When the number of angular points per shell is augmented, *S* increases, but a dip in the overlap integral for the grids with 434 angular points is observed. This can also be imputed to the frequency shift at 448 cm^{-1}, which is bigger for

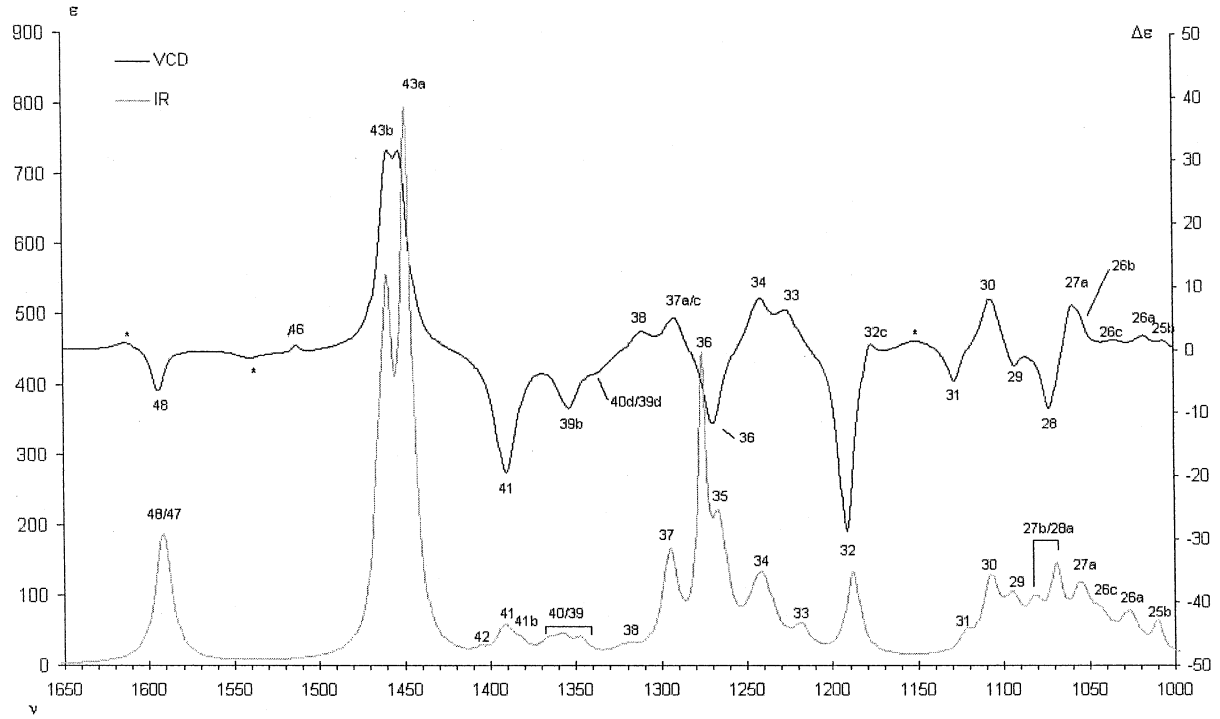

Figure 6. Lorentzian fitted unpolarized IR absorption spectrum and VCD spectrum for *R*(+)-**1**. Fundamentals are numbered based on B3LYP/6-31G* and B3LYP/cc-pVTZ calculations (absorptions and differential absorptions in absorbance units).

the 434 than for the 302 and 974 angular point grids, resulting in a poorer overlap for the 434 angular point grids. When looking at the quality of the least-squares fitting (correlation coefficient) of the dipole and rotational strength with respect to the reference grid it is seen that the effect of the 448 cm^{-1} artifact is absent. The performance of the 75 and 99 radial shell grids is alike. Pruned grids with 50 and 75 shells have also similar performances compared to those of the nonpruned versions. The (35,110)p grid shows only poor agreement with the (99,974) grid.

The computational cost is an important parameter in the applicability of a method. In Table 7 the relative CPU times for the calculation of the spectroscopic properties for the conformation eqGg′ are given where the GAUSSIAN98 default, i.e., (75,302)p, has the value of unity. Naturally the CPU load increases when the grid becomes denser. The (75,302)p and (75,302) grids give virtually the same results as well as the (50,194)p and (50,194) grids (discussed above), however, with less CPU load for the pruned grids; 0.7 against 1.8 for the (50,194) type grid and 1.0 against 3.7 for the (75,302) type grid.

The (50,194)p VCD spectrum of conformer eqGg′ is shown in Figure 4 along with the (99,974) spectrum for the 1000−1650 cm^{-1} interval. Agreement with the reference grid, as seen and discussed above, is still very good, with an overlap integral of 0.99 for this frequency interval. With the former grid the computational cost is reduced by 30% compared to the (75,302)p GAUSSIAN98 default, for the molecule studied in this paper.

One of the fundamental mathematical problems with numerical integration using a finite grid is that the rotational invariance can be lost.[24] Rotation of the molecule as a whole leaving the grid axes unrotated may cause a change in the computed energy which is naturally unphysical. This effect is even more pronounced with derivative calculations, such as the calculation of harmonic frequencies, in particular the frequencies of low-lying vibrational modes.[25]

TABLE 9: Relative B3LYP/6-31G* and B3LYP/cc-pVTZ Enthalpies (ΔH^0, in kcal/mol) and Boltzmann Populations (%F) (T = 298.15 K) for the (75,302)p Grid

	6-31G*		cc-pVTZ	
conformation	ΔH^0	%F	ΔH^0	%F
eqG′g	0.00	73.13	0.00	55.44
eqGg′	0.79	19.25	0.52	23.09
axGg′	1.57	5.19	0.99	10.48
eqTt	2.32	1.46	1.12	8.44
axTt	2.83	0.61	1.82	2.56
eqG′t	3.35	0.25		
axG′g	4.22	0.06		
eqGt	4.63	0.03		
axGt	5.15	0.01		

The single point energy, harmonic frequencies, dipole and rotational strength were calculated for three different orientations of the eqG′g B3LYP/6-31G* equilibrium geometry; the standard orientation rotated by respectively 10° and 20° about the *x* axis (10*x* and 20*x*), and the standard orientation successively rotated by 20° about the *x* axis and 30° about the *y* axis (20*x*30*y*). These calculations were performed for the (75,302)p and (50,194)p grids.

As can be seen in Table 8, for both grids, the relative energies are not rotational invariant. For the (50,194)p grid there is a rather large effect on the relative energy for orientation 20*x*30*y*, i.e., 0.1079 kcal/mol compared to the standard orientation. This behavior is undesirable, because of the significant influence on the conformational populations. The energy differences for the (75,302)p grid are on the order of 10^{-3} kcal/mol, which is not significant for our purposes.

The dipole and rotational strengths are not rotationally invariant for both grids, but differences with the standard orientation are minimal. This is shown in Table 8 where the correlation coefficients of the dipole and rotational strength with respect to the standard orientation are given. For the (50,194)p grid there is one significant sign inversion for orientation *20x* at approximately 477 cm^{-1} (mode 10a: O−H and pyridine out-of-plane bending vibration). The (75,302)p grid does not show

TABLE 10: Assignment of the Experimental Peaks Based on the B3LYP/6-31G* Calculated Spectra[a]

	experiment			B3LYP/6-31G*		
fundamental	frequency	*D*	*R*	frequency[b]	*D*	*R*
25b	1009.98	41.19	2.37	1012.51	12.06	1.30
26a	1026.19	97.63	7.61	1026.95	24.46	11.33
	1043.26	94.67	7.21			
26b	1054.93	142.70	7.21	1049.20	0.06	−1.71
27a	1059.53	-	23.28	1049.34	19.78	59.78
27b			−36.47	1059.19	20.39	−10.35
28a	1069.07	120.22		1063.90	63.47	−19.45
28b	1081.27	88.44		1067.90	6.74	2.67
29c	1094.70	114.74	−10.10	1082.90	2.01	−2.52
29a				1087.83	11.80	−5.08
29b				1087.89	3.75	−2.20
30b	1107.59	149.14	35.89	1095.25	6.43	0.71
30a				1095.84	34.04	−1.93
31b	1122.07	21.95	−17.67	1108.79	1.78	−1.87
31a				1111.05	10.06	−41.61
	1151.16		13.58			
32c	1187.96	138.10	11.23	1170.11	2.64	10.27
32a	1191.43		−98.52	1180.59	26.02	−122.52
32b				1181.27	5.64	−10.66
33c	1218.25	41.32	28.68	1199.93	0.23	−1.90
33b				1207.86	5.30	2.01
33a				1211.08	18.45	2.54
34a	1241.47	229.52	33.81	1236.60	9.52	21.38
34b				1240.77	2.51	2.09
35c	1265.98	210.45		1261.93	12.40	−2.17
35a				1267.19	4.81	−9.59
35b				1268.06	23.27	6.39
36b	1275.65	244.56	−46.67	1272.30	18.24	0.81
36a				1274.97	232.39	−31.60
37b		169.61		1280.50	19.79	−6.06
37a	1294.65		21.69	1290.68	4.00	20.36
37c				1294.57	3.22	1.10
38b	1321.13	25.34	12.31	1303.33	4.13	0.89
38a				1308.63	7.03	1.08
	1336.03		−9.15	1341.16	0.67	−2.47
39a				1344.93	16.80	0.15
39b	1347.16	23.20	−34.64	1350.40	3.46	−6.44
40a	1357.45	26.42		1356.42	0.73	9.09
40c	1365.61	25.89		1362.71	3.28	−0.32
40b	1383.48	24.14		1369.45	13.33	10.53
41b	1391.62	41.49	−78.20	1381.98	2.36	−8.85
41a				1392.64	52.83	−90.56
42a				1395.46	31.54	0.40
42b	1405.91	5.16		1410.69	15.81	8.27
43a	1448.25	556.84	63.91	1448.47	261.14	67.22
43b	1459.64	402.54	64.16	1449.18	62.99	9.21
44a				1458.61	3.10	−2.24
44b				1459.40	3.51	−0.07
45b				1474.28	2.06	0.48
45a				1474.41	0.32	0.67
46b	1512.77		1.58	1481.38	0.93	−0.19
46a				1481.68	9.00	2.73
	1540.29		−5.04			
47a				1581.99	35.64	4.80
47b				1582.11	9.05	1.27
48a	1591.44	190.67	−13.05	1596.76	3.56	−20.54
48b				1597.21	1.08	−4.76
	1612.72		5.15			

[a] The experimental values of the vibrational frequencies (in cm^{-1}), dipole (*D* in 10^{-40} esu^2 cm^2), and rotational strength (*R* in 10^{-44} esu^2 cm^2) were calculated by Lorentzian fit. Fundamentals are addressed according to the minimum (a ≡ eqG′g, b ≡ eqGg′, c ≡ axGg′). Calculated values of *D* and *R* are Boltzmann weighed according to Table 9. [b] Scaled with factor 0.9669.

TABLE 11: Assignment of the Experimental Peaks Based on the B3LYP/cc-pVTZ Calculated Spectra[a]

	experimental			B3LYP/cc-pVTZ		
fundamental	frequency	*D*	*R*	frequency[b]	*D*	*R*
25b	1009.98	41.19	2.37	1008.86	17.22	5.12
26a	1026.19	97.63	7.61	1026.02	19.50	12.67
26c	1043.26	94.67	6.16	1042.17	3.97	4.91
27a	1054.93	142.70	23.28	1051.61	27.95	46.92
26b				1053.28	10.00	1.73
27b				1056.24	13.80	−22.82
28a	1069.07	120.22	−36.47	1067.22	38.40	−25.99
28b				1072.95	9.53	4.12
29c	1081.27	88.44	−10.10	1083.04	5.96	−4.02
29a	1094.70	114.74		1090.90	10.65	−27.37
29b				1092.15	1.42	−1.38
	1151.16		13.58			
30b	1107.59	149.14	35.89	1096.77	11.17	−1.87
30a				1098.21	27.33	24.69
30c				1107.88	3.04	−0.29
31b	1122.07	21.95	−17.67	1115.01	2.39	−1.14
31a				1116.77	8.13	−37.30
32c	1187.96	138.10	11.23	1173.59	5.17	20.20
32a			−98.52	1182.12	21.38	−90.57
32b				1182.82	7.73	−9.08
33c	1218.25	41.32	28.68	1202.75	0.89	−4.40
33b				1211.84	5.42	4.34
33a				1216.52	13.59	0.49
34d				1225.00	1.91	−6.57
34a	1241.47	229.52	33.81	1239.74	15.19	26.68
34b				1244.00	5.84	5.42
35b	1265.98	210.45		1269.88	67.63	4.55
35a				1271.07	13.14	−14.62
36a	1275.65	244.56	−46.67	1272.86	160.95	−24.13
36b				1273.78	0.88	0.25
37b	1294.65	169.61	21.69	1281.39	3.37	−3.58
37a				1289.93	18.80	12.71
37c				1295.11	6.97	2.36
38b	1321.13	25.34	12.31	1301.14	13.59	−1.70
38a				1309.50	9.74	5.65
39d				1325.31	0.48	−0.77
40d	1336.03		−9.15	1341.16	0.67	−2.47
39a	1347.16	23.20		1343.97	6.62	−0.10
39b	1357.45	26.42	−9.15	1349.38	3.43	−7.18
40a	1365.61	25.89	−34.64	1357.47	1.37	2.31
40b	1383.48	24.14		1367.40	12.48	10.20
41b	1391.62	41.49		1380.81	1.66	−8.74
41a			−78.20	1387.41	41.61	−59.24
42a				1393.07	6.04	−7.99
42b	1405.91	5.16		1405.00	12.44	7.29
43a	1448.25	556.84	63.91	1449.81	207.16	46.17
43b	1459.64	402.54	64.16	1450.52	78.24	10.90
44b				1461.33	5.60	2.29
44a				1461.84	1.34	4.52
45a				1464.95	0.45	1.50
45b				1465.94	0.86	1.24
46b	1512.77		1.58	1474.35	5.17	−1.57
46a				1476.59	12.85	0.02
	1540.29		−5.04			
47a				1584.80	26.11	3.30
47b				1585.11	10.42	1.15
48a	1591.44	190.67	−13.05	1597.13	4.46	−12.38
48b				1598.00	2.12	−4.76
	1612.72		5.15			

[a] The experimental values of the vibrational frequencies (in cm^{-1}), dipole (*D* in 10^{-40} esu^2 cm^2), and rotational strength (*R* in 10^{-44} esu^2 cm^2) were calculated by Lorentzian fit. Fundamentals are addressed according to the minimum (a ≡ eqG′g, b ≡ eqGg′ c ≡ axGg′, d ≡ eqTt). Calculated values of *D* and *R* are Boltzmann weighed according to Table 9. [b] Scaled with factor 0.9779.

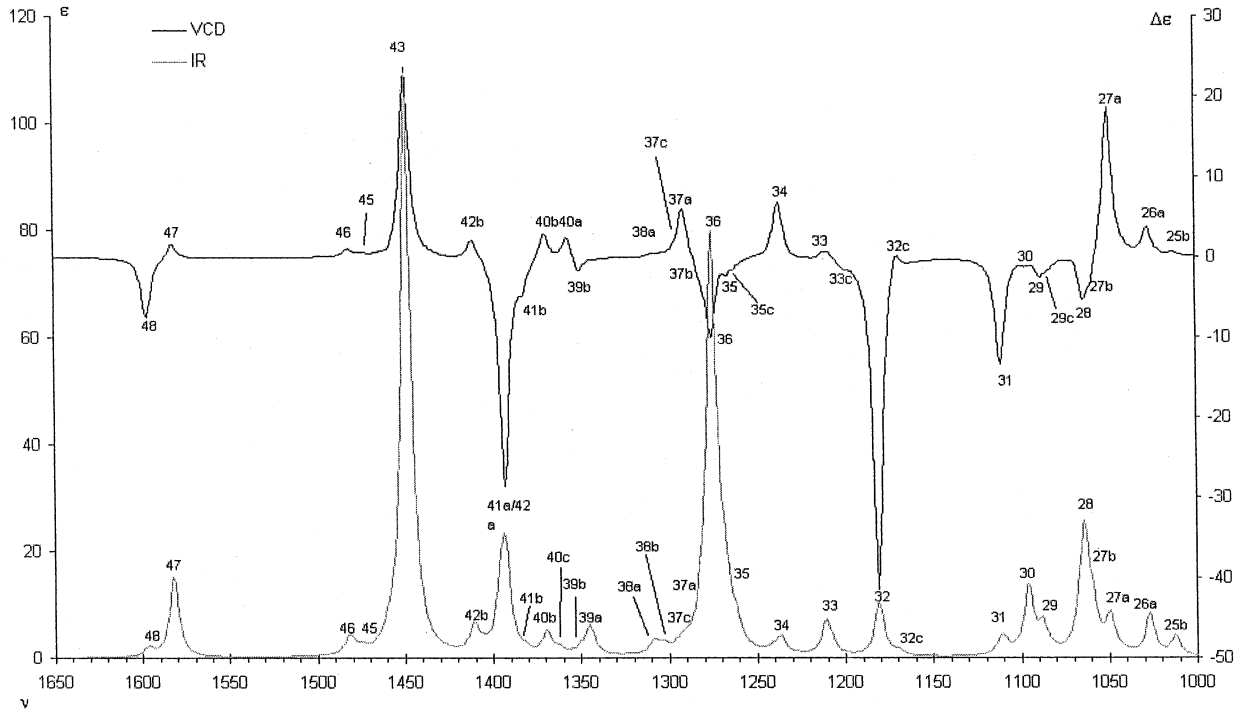

Figure 7. B3LYP/6-31G* simulated (based on all conformations) unpolarized IR absorption spectrum and VCD spectrum (IR intensities in 10^{-40} esu^2 cm^2, VCD intensities in 10^{-44} esu^2 cm^2, frequencies in cm^{-1}).

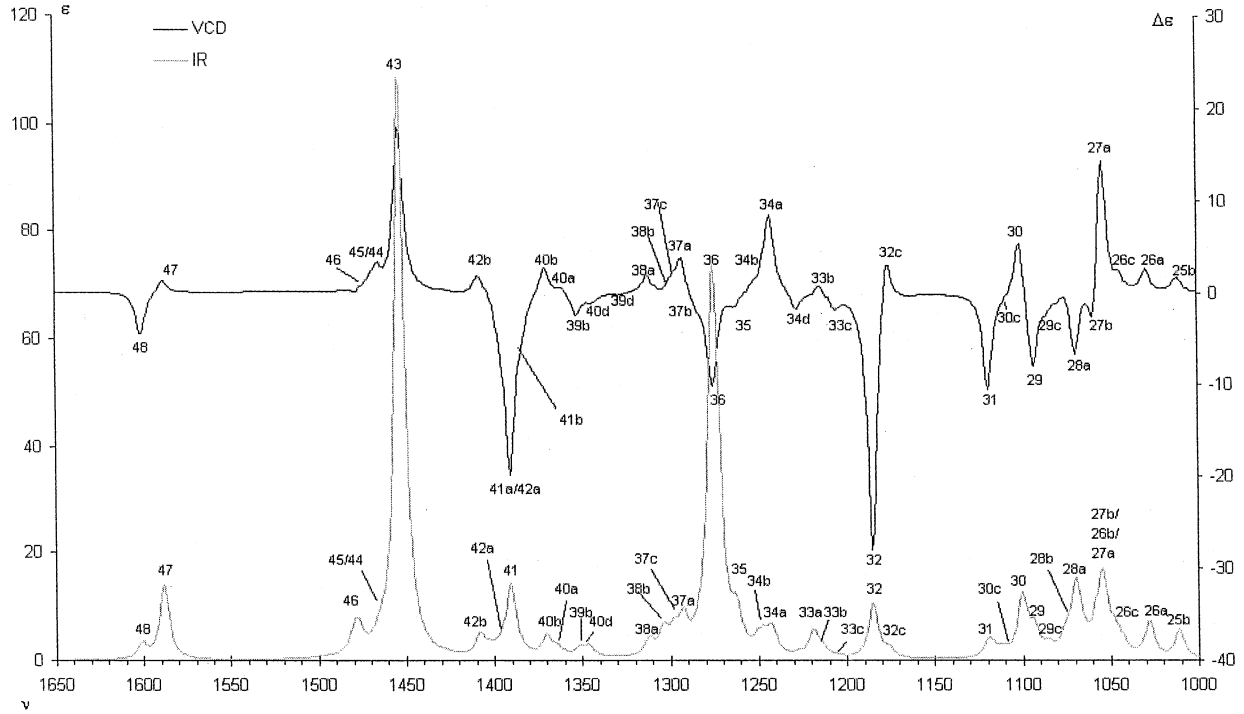

Figure 8. B3LYP/cc-pVTZ simulated (based on the five lowest energy conformers) unpolarized IR absorption spectrum and VCD spectrum (IR intensities in 10^{-40} esu^2 cm^2, VCD intensities in 10^{-44} esu^2 cm^2, frequencies in cm^{-1}).

any significant sign inversions. In Table 8 the overlap integrals of the IR and VCD spectra are given for the different orientations relative to the standard orientation. This is done for two frequency intervals, i.e., 300−2000 cm^{-1} and 1000−2000 cm^{-1}. It can be seen that the (50,194)p overlap integrals are larger for the 1000−2000 cm^{-1} interval. This is because of the poor agreement of the low vibrational frequencies discussed above. For the 1000−2000 cm^{-1} interval there are very small differences between the spectra from the different orientations, but not significant. The (75,302)p spectra are virtually rotationally invariant for the 1000−2000 cm^{-1} interval. The (75,302)p vibrational frequencies beneath 500 cm^{-1} are not rotationally invariant, and if these are in the scope of interest, a denser grid should be used.

In Figure 5 the (75,302)p B3LYP/6-31G* single conformer spectra of conformers eqGt and eqGg′ are shown. They differ in energy by 4.15 kcal/mol. Geometrical differences are minimal except for one dihedral angle τ_3 ($\Delta\tau_1 = 2.0/\Delta\tau_2 = 15.1/\Delta\tau_3 =$

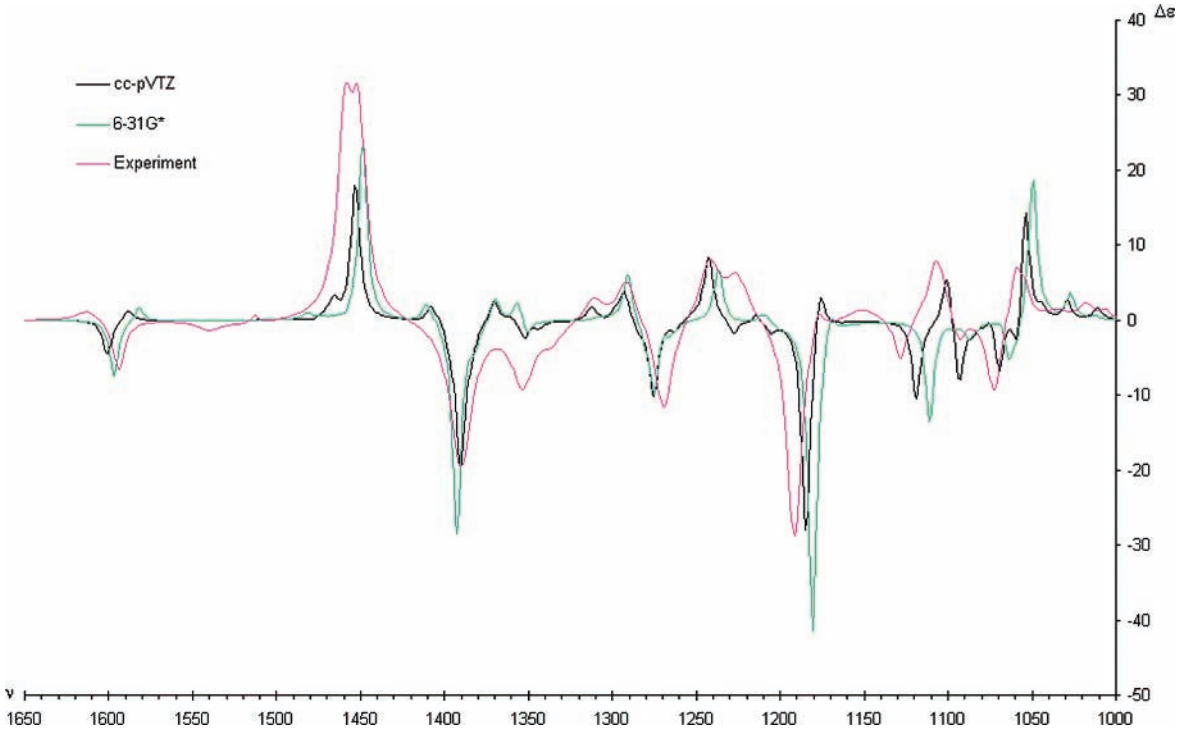

Figure 9. B3LYP/6-31G* (green, based on all conformations) and B3LYP/cc-pVTZ (black, based on the five lowest energy conformations) simulated VCD spectra together with the experimental spectrum (pink) for *R*(+)-**1** (intensities in 10^{-44} esu^2 cm^2 and absorbance units, frequencies in cm^{-1}).

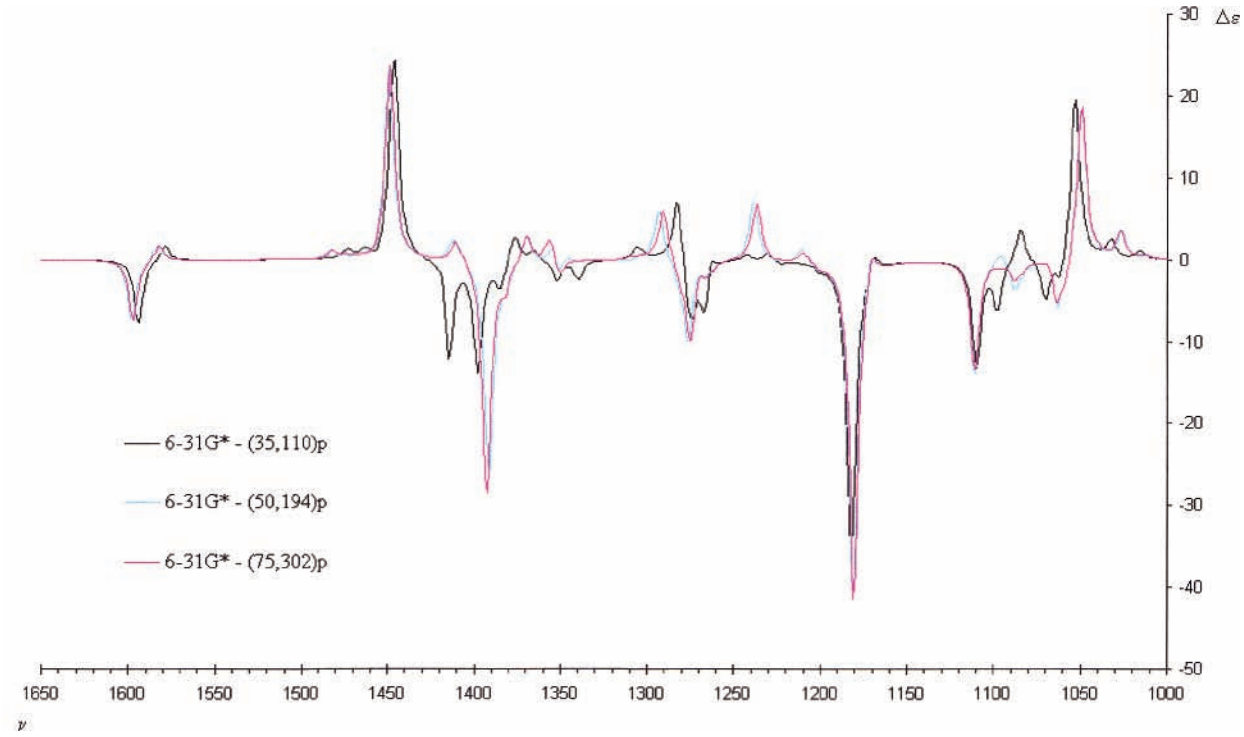

Figure 10. Simulated B3LYP/6-31G* VCD spectra calculated with following grids: (35,110)p (black), (50,194)p (blue), and (75,302)p (pink) (VCD intensities in 10^{-44} esu^2 cm^2, frequencies in cm^{-1}).

108.9). The VCD spectra, however, are very different. Some transitional frequencies are shifted and multiple peak inversions are seen (fundamental 32−35). This emphasizes the need for thorough conformational analysis, even for relatively rigid molecules such as **1**.

Multiple Conformations. In Figure 6 the Lorentzian fitted experimental IR absorption and VCD spectra are given for *R*(+)-**1**. Every peak is fitted to a Lorentzian type band, with variable width. The peak numbering is based on the simulated (Boltzmann weighted) B3LYP/6-31G* and B3LYP/cc-pVTZ calculations.

Table 9 gives Boltzmann populations for all minima, calculated using the 6-31G* and cc-pVTZ basis sets and the (75,302)p grid. The major contributions to the 6-31G* IR absorption and VCD spectra are from eqG′g, eqGg′, and axGg′ conformations.

The 6-31G* basis set is often used as a sufficiently good basis set for VCD calculations.[6] Using eq 3 for the experimental

TABLE 12: Maximized Overlap Integrals S_{max} and Optimal Scaling Factor σ_{max} for the Simulated Spectra Calculated with Various Basis Sets with Respect to the Experimental Spectrum

		6-31G*	6-31G**	6-311G**	cc-pVDZ	cc-pVTZ
IR	S_{max}	0.848	0.862	0.852	0.863	0.855
	σ_{max}	0.9669	0.9688	0.9792	0.9740	0.9779
VCD	S_{max}	0.594	0.615	0.619	0.559	0.701
	σ_{max}	0.9729	0.9764	0.9846	0.9841	0.9824

TABLE 13: Maximized Overlap Integrals S_{max} and Optimal Scaling Factor σ_{max} for the Simulated Spectra Calculated with Various Grids with Respect to the Experimental Spectrum

grid	S_{max} IR	σ_{max}	S_{max} VCD	σ_{max}
(35,110)p	0.850	0.9682	0.615	0.9727
(50,194)p	0.851	0.9669	0.608	0.9729
(75,302)p	0.848	0.9669	0.594	0.9729
(50,302)	0.850	0.9669	0.599	0.9732
(75,194)	0.849	0.9669	0.598	0.9736
(75,434)	0.849	0.9669	0.591	0.9729
(99,302)	0.852	0.9669	0.593	0.9729

and the broadened IR absorption 6-31G* spectrum, an optimized scaling factor of 0.9669 (yielding an IR absorption overlap integral of 0.85) was found. This agrees very well with the scaling factor cited in the literature, being 0.9614.[26]

The absolute values of the experimental dipole strengths, given in Table 10, do not agree with the calculated. Nevertheless a proportional agreement is seen. Also, most of the experimental peaks correspond with more than one calculated peak. Despite these facts, there is a good agreement between the spectra and most of the experimental peaks can be assigned (Table 10). Experimental IR absorption peaks 39 and 40 are not clearly resolved but have small intensities. The experimental spectrum shows a doublet for the 43 mode. Most peaks from the experimental VCD spectrum can be assigned based on the 6-31G* calculations (Table 10). Because of the limited resolution, some modes are not visible. Good agreement is seen between the calculated ones and the experimental rotational strengths. Some experimentally observed peaks cannot be assigned, i.e., the peak between 26b and 26a, the one between 31 and 32c, between 38 and 39b, between 48 and 46, and the one left to 48. Peaks 30 and 26b have the wrong sign, as can be seen in Table 10 and Figure 7.

To find the reason for these peak inversions, particularly for mode 30 (being the only visible inversion), B3LYP/cc-pVTZ IR absorption and VCD spectra were also simulated and are given in Figure 8. The peak assignment is given in Table 11. A salient characteristic is that there are more visible peaks compared to the 6-31G* spectrum. One of the reasons is that the energy separation between the minima is smaller, consequently giving higher populations for the local minima (Table 9). Peaks of the eqTt conformation are visible, which was not the case for the 6-31G* spectrum. The frequency scaling factor was determined to be 0.9779 (yielding an IR absorption overlap integral of 0.86).

All experimental IR absorption and VCD peaks can be assigned based on the cc-pVTZ spectrum, again except for modes 39 and 40 (Table 11 and Figure 8). The peak in the experimental IR absorption spectrum that could not be assigned based on the 6-31G* spectrum corresponds with the B3LYP/cc-pVTZ 26c mode. Other small differences between the IR absorption spectra for both basis sets are the intensities for peak 28a and peak 42a. The negative experimental VCD peak between 38 and 39b agrees with the coincidental cc-pVTZ 39d and 40d modes. Again the experimental VCD peak between peaks 32c and 31, between peaks 46 and 48 and the one left from peak 48 cannot be assigned. When one has a closer look at mode 30, one sees that there is no longer a peak inversion compared to the experiment. The overall agreement of the cc-pVTZ simulated VCD spectrum compared with the experimental spectrum is very good.

The overlap integrals for the 6-31G* and cc-pVTZ VCD spectra with the experimental are respectively 0.59 and 0.70. These spectra are shown together in Figure 9. Based on this agreement between the calculated spectrum (which was simulated for the *R* configuration) and the experimental spectrum, the absolute configuration of the (+)-sample was determined as *R*. This agrees with the knowledge based on retro-synthesis. Due to the fact that it was not known to the computational chemist what experimental spectrum corresponded to what enantiomer, the correct assignment allows for the conclusion that DFT calculations are a powerful tool in determining the chirality of a molecule.

The influence of basis sets and grids on the single conformer IR absorption and VCD spectra is discussed above. For the basis sets listed in Table 2 the Boltzmann weighed spectra were calculated and compared with experiment, i.e., the overlap integral *S* between simulated and experimental spectra was maximized, by scaling the calculated frequencies, for the 1000−1650 cm^{-1} frequency interval. Results are given in Table 12. The overlap integrals for the IR absorption spectra do not change much. For the VCD spectra there is a clear increase of the overlap integral with the basis set, especially for the cc-pVTZ basis set. This is probably due to 2 different effects. The first are the lower conformational energies compared to 6-31G*, which cause that in the simulated cc-pVTZ spectrum more peaks appear, giving a better agreement with the experimental spectrum. A second reason is probably the inherently better quality of the cc-pVTZ VCD characteristics.

Weighted spectra were also calculated with the grids given in Table 4 and the 6-31G* basis set. The 1000−1650 cm^{-1} part of these spectra were compared with the experiment of which the results are given in Table 13. The IR overlap integrals for the different grids are virtually the same. A surprisingly, but fortuitously high VCD overlap integral for the (35,110)p grid is found. In Figure 10 the simulated VCD spectra for the pruned grids are depicted. One can clearly see that some (35,110)p grid peaks are inverted i.e., peaks corresponding with modes 29 and 42b. Nonetheless the (50,194)p and (75,302)p VCD spectra differ very little, the slight augmented overlap integral value for the (50,194)p grid is due to a peak inversion [compared to the (75,302)p grid] of mode 30 toward the experimental spectrum. This is certainly not an indication that the sparse (50,194)p grid performs better than denser grids. On the contrary, the agreement in sign of mode 30 with the experiment is merely coincidental.

Although it seems that the smaller (50,194)p grid performs similarly to the larger (75,302)p grid, care must be taken not to take this as a general feature for any molecule. Many more molecules need to be considered in order to establish whether this is generally valid. It was, however, found that the individual VCD spectra show only minor differences between the different grids, except for the smallest grid, i.e., (35,110)p. The good agreement and correct assignment based on the (50,194)p grid may be fortuitous, since the use of a smaller grid may well cause several errors, that may possibly cancel each other. A similar argument may be formulated for basis sets.

From previous results, it has been found that the 6-31G* basis set performs sufficiently well with the B3LYP functional and

(probably) the (75,302)p grid. Even though this is widely accepted as a good level of calculation, even there some validation should be done by performing calculations with larger basis sets and denser grids.

Conclusions

This study shows that VCD spectroscopy in combination with DFT is an excellent technique for the determination of the absolute configuration. Reducing the computational cost by varying basis set and grid size, this study showed that the 6-31G basis set is too small to produce good spectra. The 6-31G* basis set is an acceptable basis set, and cc-pVTZ yields the best agreement. The small (35,110)p grid also gives inferior results. The (50,194)p grid gives good results for the simulation of VCD spectra together with 6-31G* basis set using the B3LYP hybrid density functional in this specific case. CPU cost for the calculation of the spectroscopic properties are approximately 30% less than those for the (75,302)p (standard GAUSSIAN98) grid. Although this study suggests that this grid would be an acceptable choice, several issues need to be considered. Rotational invariance may be lost, which is not only unphysical but will also influence the calculated Boltzmann distribution. This in turn then influences the calculated, Boltzmann weighted spectrum. On the other hand, VCD spectra were found to be very similar for the (50,194)p and (75,302)p grids. Naturally this conclusion needs to be checked further for more molecules to establish whether this is not due to some fortuitous cancellation of errors.

The use of the overlap integral as a quantitative measure for the similarity of VCD spectra is very useful, but one has to be careful in drawing conclusions on solely the value of the overlap integral, especially when anomalies are observed. The next step will be the tuning of this overlap index to make it proximity sensitive.

Acknowledgment. P. Bultinck acknowledges support from Ghent University and the National Fund of Scientific Research—Flanders for continued support to the quantum chemistry group.

Supporting Information Available: (75,302)p B3LYP/6-31G* VCD spectra of the five lowest minima. This material is available free of charge via the Internet at http://pubs.acs.org.

References and Notes

(1) Ariens, E. J. *Med. Res. Rev.* **1986**, *6*, 451−466.

(2) Aamouche, A.; Devlin, F. J.; Stephens, P. J. *J. Am. Chem. Soc.* **2000**, *122*, 2346−2354.

(3) Specht, K. M.; Nam, J.; Ho, D. M.; Berova, N.; Kondru, R. K.; Beratan, D. N.; Wipf, P.; Pascal, R. A.; Kahne, D. *J. Am. Chem. Soc.* **2001**, *123*, 8961−8966.

(4) Parker, D. *Chem. Rev.* **1991**, *91*, 1441−1457.

(5) Cheeseman, J. R.; Frisch, M. J.; Devlin, F. J.; Stephens, P. J. *Chem. Phys. Lett.* **1996**, *252*, 211−220.

(6) Stephens, P. J.; Devlin, F. J. *Chirality* **2000**, *12*, 172−179.

(7) Ashvar, C. S.; Stephens, P. J.; Eggimann, T.; Wieser, H. *Tetrahedron: Asymmetry* **1998**, *9*, 1107−1110.

(8) van Emelen, K.; de Bruyn, M. F. L.; Alcazar-Vaca, M. J.; Andres-Gil, J. I.; Fernandez-Gadea, F. J.; Matesanz-Ballesteros, M. E.; Bartolome-Nebreda, J. M. Preparation of dioxinopyridines and related compounds for treating impaired fundic relaxation. Patent WO 2001-EP6749[WO 2001098306].

(9) Soukri, M.; Lazar, S.; Akssira, M.; Guillaumet, G. *Org. Lett.* **2000**, *2*, 1557−1560.

(10) Polavarapu, P. L. *Spectroscopy* **1994**, *9*, 48−55.

(11) *MM3*, version 1996; obtained from QCPE.

(12) Bultinck, P.; Van Alsenoy, C.; Goeminne, A.; Van de Vondel, D. *J. Phys. Chem. A* **2000**, *104*, 11801−11809.

(13) Frisch, M. J.; Trucks, G. W.; Schlegel, H. B.; Scuseria, G. E.; Robb, M. A.; Cheeseman, J. R.; Zakrzewski, V. G.; Montgomery, J. A., Jr.; Stratmann, R. E.; Burant, J. C.; Dapprich, S.; Millam, J. M.; Daniels, A. D.; Kudin, K. N.; Strain, M. C.; Farkas, O.; Tomasi, J.; Barone, V.; Cossi, M.; Cammi, R.; Mennucci, B.; Pomelli, C.; Adamo, C.; Clifford, S.; Ochterski, J.; Petersson, G. A.; Ayala, P. Y.; Cui, Q.; Morokuma, K.; Malick, D. K.; Rabuck, A. D.; Raghavachari, K.; Foresman, J. B.; Cioslowski, J.; Ortiz, J. V.; Stefanov, B. B.; Liu, G.; Liashenko, A.; Piskorz, P.; Komaromi, I.; Gomperts, R.; Martin, R. L.; Fox, D. J.; Keith, T.; Al-Laham, M. A.; Peng, C. Y.; Nanayakkara, A.; Gonzalez, C.; Challacombe, M.; Gill, P. M. W.; Johnson, B. G.; Chen, W.; Wong, M. W.; Andres, J. L.; Head-Gordon, M.; Replogle, E. S.; Pople, J. A. *Gaussian 98*, revision A.6; Gaussian, Inc.: Pittsburgh, PA, 1998.

(14) Becke, A. D. *J. Chem. Phys.* **1993**, *98*, 5648−5652.

(15) Lee, C. T.; Yang, W. T.; Parr, R. G. *Phys. Rev. B* **1988**, *37*, 785−789.

(16) Hehre, W. J.; Radom, L.; Schleyer, P. R.; Pople, J. A. *Ab initio Molecular Orbital Theory*; Wiley: New York, 1986.

(17) Gill, P. M. W.; Johnson, B. G.; Pople, J. A. *Chem. Phys. Lett.* **1993**, *209*, 506−512.

(18) Murray, C. W.; Handy, N. C.; Laming, G. J. *Mol. Phys.* **1993**, *78*, 997−1014.

(19) Frisch, M. J.; Frisch, A. E.; Foresman J. B. *Gaussian 94 User's Reference*, 5th ed.; Gaussian, Inc.: Pittsburgh, 1995.

(20) Stephens, P. J. *J. Phys. Chem.* **1985**, *89*, 748−752.

(21) Stephens, P. J. *J. Phys. Chem.* **1987**, *91*, 1712−1715.

(22) McQuarrie, D. A. *Statistical Thermodynamics*; Harper and Row: New York, 1973.

(23) Schellman, J. A. *Chem. Rev.* **1975**, *75*, 323−331.

(24) Johnson, B. G.; Gill, P. M. W.; Pople, J. A. *Chem. Phys. Lett.* **1994**, *220*, 377−384.

(25) Johnson, B. G.; Frisch, M. J. *Chem. Phys. Lett.* **1993**, *216*, 133−140.

(26) Scott, A. P.; Radom, L. *J. Phys. Chem.* **1996**, *100*, 16502−16513.